Received August 16, 2019, accepted September 12, 2019, date of publication September 18, 2019, date of current version October 2, 2019.

Digital Object Identifier 10.1109/ACCESS.2019.2942070

Structure-Aware Interrupted SAR Imaging Method for Change Detection

YI GAN[1], XUNCHAO CONG[1], AND YUE YANG[2], (Student Member, IEEE)

[1]The 10th Research Institute of CETC, Chengdu 610036, China
[2]School of Information and Communication Engineering, University of Electronic Science and Technology of China, Chengdu 611731, China

Corresponding author: Yue Yang (yueyangmoon7@163.com)

ABSTRACT By exploiting the continuity structure of target scene, the problem of interrupted synthetic aperture radar (SAR) imaging for change detection is studied in this paper. Timeline constraints imposed on multi-function modern radars lead to gapped SAR data collections, which in turn results in corrupted image that degrades reliable coherent change detection (CCD). In this paper we extrapolate the missing data using the sparse Bayesian framework. In particular, the inherent clustered structures of the sparse target scene are characterized by structure-aware Bayesian priors. The variational Bayesian inference (VBI) is then utilized to estimate an approximated posterior of the sparse coefficients. Finally the CCD images are obtained by applying the coherence estimator to the resultant complex images. Based on the structural information in the imaging process, the devised method offers the advantages of preserving the weak scatterers and suppressing the artificial points with fewer measurements. Experimental results are presented to demonstrate the effectiveness and superiority of the proposed algorithm.

INDEX TERMS Synthetic aperture radar (SAR), change detection, continuity structure, variational Bayesian inference (VBI).

I. INTRODUCTION

The emerging synthetic aperture radar (SAR) technique has been widely utilized in military and civilian applications in the past decades. Multi-mode operation is supported by the airborne radar systems such as searching, tracking and automatic target recognition, resulting in data gaps in the coherent SAR collections [1]–[3]. Such gapped data (often known as interrupted SAR) manifest as leakage artifacts and seriously affect the resulting conventionally formed SAR image.

Considerable efforts have been made to deal with missing data in SAR image formation processing. The matched-filtering based imaging method is implemented by setting the missing samples to zero and then performing fast Fourier transform (FFT). Nevertheless, the drawback of this method is the poor resolution, which is especially serious in the gapped data case. Recently, sparse signal recovery from the field of compressive sensing (CS) [4] has emerged as a promising technique to address the interrupted SAR imaging problem. For the sake of ''filling-in'' the gaps in the SAR spectrum, this technique makes assumptions about the sparsity of the underlying image. Work in this category includes two main strategies. The first one is the relaxation strategy. It approximates the original NP-hard problem by ℓ_p-norm minimization problem with $0 < p \leq 1$, e.g., basis pursuit (BP) [5], least absolute shrinkage and selection operator (LASSO) [6], and focal underdetermined system solver (FOCUSS) [7], [8]. The other approach is composed of iterative greedy algorithms with $p = 0$. Such methods include orthogonal matching pursuit (OMP) [9], and compressive sampling matching pursuit (CoSaMP) [10].

SAR change detection performance becomes important in the case of multi-pass data processing. In [11]–[13], the change detection problem in different reference and mission interrupt patterns was studied. The authors considered both the ℓ_1 regularized estimator based independently processing method [12] and the group sparsity (GS) algorithm based jointly processing method [13]. After SAR image formation, typical change detection algorithms were implemented. In the case of independent processing of each data, the weak scatterers in the target scene may not be well-preserved and the back ground noise may not be properly shrunk only with a simple sparsity constraint. In contrast, the joint reconstruction is shown to enhance the performance

The associate editor coordinating the review of this manuscript and approving it for publication was Jinming Wen.

gains because of the introducing of common spatial reflectivity support constraints in the multi-pass data processing.

To further improve the performance of radar imaging, the inherent structures of targets underlying sparsity patterns are considered by placing block or cluster structural information on the scatterers. Over the past years, quite a number of approaches for block sparse signal recovery have been developed. For instance, the block-OMP method [14] and the group LASSO method [15] are able to obtain enhanced reconstruction performance in the block sparse signals case. In these methods, the groups or blocks of the sparse coefficients are pre-specified, but the prior information about the block partition of coefficients is often practically unavailable. Another type of methods is based on the Bayesian framework that can flexibly provide structured priors in a probabilistic manner, including pattern-coupled sparse Bayesian learning (PC-SBL) [16], [17], Cluss-MCMC/-VB [18]–[21] and so on. Unfortunately, these Bayesian algorithms are only applicable for a specific type of structures.

To tackle the above problems, in this paper, a general structure-aware interrupt SAR imaging method is developed under the Bayesian framework, with the goal of achieving reliable change detection. Particularly, the inherent clustered structures of scatterers are introduced through a Beta-Bernoulli process, avoiding the demand of the precise model of the structures. Because the resulted posterior distribution of the structure-aware sparse Bayesian model cannot be analytically obtained, this paper resorts to the variational Bayesian inference (VBI) [22], [23] to estimate the approximated posterior of the coefficient vectors. Finally the CCD results are achieved based on the performance-improved SAR imagery. By making use of the continuity information of the target scene in the imaging procedure, the proposed method offers the advantages of preserving the weak scatterers and removing the artificial points with fewer measurements.

The remaining sections of this paper are organized as follows. In Section II, we briefly introduce the Bayesian model for interrupted SAR imaging. The efficient inferences of the latent variables and parameters via VBI are given in Section III. Representative simulations are carried out in Section IV, and at last, we make a conclusion in Section V.

II. BAYESIAN MODEL FOR INTERRUPTED SAR IMAGING

In this section, the interrupted SAR imaging model is first presented. On this basis, we employ the Bayesian structured sparsity prior to enforce the continuity of target scene, followed by the prior on noise precision to facilitate the Bayesian inference.

A. INTERRUPTED SAR OBSERVATION MODEL

A spotlight-mode SAR observation model is considered here. Under the high-frequency hypothesis [24], the superposition of the responses from U individual scattering centers is used to approximate the composite scattering response of the target scene. As a result, we can write down the phase history as

$$r(\rho,\phi)=\sum_{u=1}^{U}\alpha(x_u,y_u)\exp\{-j2\rho(x_u\cos\phi+y_u\sin\phi)\} \quad (1)$$

where $\rho = 2\pi/\lambda$ represents the spatial frequency, λ is the wavelength, ϕ denotes the aspect angle, and $\alpha(x_u, y_u)$ is the scattering coefficient of the scattering center at the position of (x_u, y_u). Assume that the target scene of interest is discretized into an $M \times N$ grid in the cross-range and range domains. Then each scattering center located at grid (m, n) is represented by (x_m, y_n) with amplitude $\alpha(x_m, y_n)$. In particular, x_m is in the range of $(-\frac{M\delta_a}{2} : \delta_a : \frac{M\delta_a}{2} - \delta_a)$ and y_n belongs to $(-\frac{N\delta_r}{2} : \delta_r : \frac{N\delta_r}{2} - \delta_r)$, with δ_a and δ_r standing for the cross-range resolution and range resolution, respectively. On this basis, the over-complete dictionary Θ sized $L \times MN$ is constructed with the element defined as $\Theta_{m,n}(l) = \exp\{-j2\rho_l(x_m\cos\phi_l + y_n\sin\phi_l)\}$. Denote the coefficient vector by $\boldsymbol{\alpha} = [\alpha_{1,1}\ldots\alpha_{m,1}, \alpha_{1,2}\ldots\alpha_{1,n}\ldots\alpha_{m,n}]^T$. Thus, the mathematical model can be described as follows:

$$\mathbf{r} = \Theta\boldsymbol{\alpha} + \boldsymbol{\zeta} \quad (2)$$

where $\boldsymbol{\zeta}$ denotes the additive noise.

Furthermore, for interrupted SAR data collections, frequency notching of the transmitted pulse leads to the SAR spectrum gaps in the range direction, while irregular azimuth coordinates of pulse transmissions results in the SAR spectrum gaps in the azimuth dimension. The CCD problem is considered by monitoring the same ground area and processing the measurements obtained at different observation time, i.e., a reference pass and a mission pass (symbolized s and t, respectively). As we know, only L^η out of L data samples are available in interrupted SAR observation, where the superscript $\eta \in \{s, t\}$, and each data may be measured in different interrupt patterns. Consequently, the resulting interrupted SAR observation model is written as

$$\mathbf{r}^\eta = \Theta^\eta\boldsymbol{\alpha}^\eta + \boldsymbol{\zeta}^\eta \quad (3)$$

where $\mathbf{r}^\eta \in \mathbb{C}^{L^\eta}$ is the associated ηth pass noisy measurements, $\Theta^\eta \in \mathbb{C}^{L^\eta \times MN}$ represents the dictionary corresponding to the ηth pass interrupt pattern, $\boldsymbol{\alpha}^\eta \in \mathbb{C}^{MN}$ and $\boldsymbol{\zeta}^\eta \in \mathbb{C}^{L^\eta}$ denote the spatial reflectivity and the noise in the ηth pass collection, respectively. In general, $\boldsymbol{\zeta}^\eta$ could be supposed as zero-mean complex Gaussian distribution. Using this hypothesis, the conditional distribution for the observation $\boldsymbol{r}^\eta$ is given by

$$p(\mathbf{r}^\eta|\Theta^\eta\boldsymbol{\alpha}^\eta, \beta^\eta) = \mathcal{CN}(\mathbf{r}^\eta|\Theta^\eta\boldsymbol{\alpha}^\eta, 1/(\beta^\eta)\mathbf{I}) \quad (4)$$

where β^η is the ηth pass noise precision.

B. BAYESIAN STRUCTURED SPARSITY PRIOR

Taking the sparsity of the coefficient vector $\boldsymbol{\alpha}^\eta$ into consideration, we use the formula $\boldsymbol{\alpha}^\eta = \mathbf{d}^\eta \odot \mathbf{g}^\eta$ to separate the signal support $\mathbf{g}^\eta$ from the coefficient vector $\boldsymbol{\alpha}^\eta$, where $\odot$ denotes

the point wise multiplication. Similar to [21], we utilize the hierarchical prior for $\mathbf{d}^\eta$ to enhance the sparsity of $\mathbf{d}^\eta$, i.e.,

$$p\left(\mathbf{d}^\eta|\boldsymbol{\sigma}^\eta\right) = \mathcal{CN}\left(\mathbf{d}^\eta|\mathbf{0}, 1/\Sigma^\eta\right) = \prod_{v=1}^{MN} p\left(d_v^\eta|\sigma_v^\eta\right) \tag{5}$$

where $\Sigma^\eta = \text{diag}(\boldsymbol{\sigma}^\eta)$ is the matrix of the precision parameters with $\boldsymbol{\sigma}^\eta = [\sigma_1^\eta, \sigma_2^\eta, \ldots, \sigma_{MN}^\eta]^T$. Then we place a Gamma prior on σ_v^η with parameters a^η and b^η, namely,

$$p\left(\sigma_v^\eta\right) = \text{Gamma}\left(\sigma_v^\eta|a^\eta, b^\eta\right). \tag{6}$$

The overall prior on $\mathbf{d}^\eta$ with respect to model parameters a^η and b^η is computed analytically via integrating over $\boldsymbol{\sigma}^\eta$

$$\begin{aligned} p(\mathbf{d}^\eta|a^\eta, b^\eta) &= \int p(\mathbf{d}^\eta|\boldsymbol{\sigma}^\eta)p(\boldsymbol{\sigma}^\eta|a^\eta, b^\eta) \\ &\propto \prod_{v=1}^{MN}\left(b^\eta + (d_v^\eta)^2\right)^{-(a^\eta+1)}. \end{aligned} \tag{7}$$

It is observed that (7) corresponds to the Student-t distribution [25]. By choosing proper value of a^η and b^η, the Student-t distribution can be strongly peaked about $\mathbf{d}^\eta = \mathbf{0}$. Hence the overall prior on $\mathbf{d}^\eta$ favours sparseness.

In spite of the sparsity, the scattering distribution of a practical target scene also shows strong continuity characteristic. We consider a Bernoulli distribution with parameter $\boldsymbol{\gamma}^\eta$ on the signal support $\mathbf{g}^\eta$ to enforce the continuity structured prior, i.e.,

$$p(g_v^\eta) = \text{Bernoulli}(\gamma_v^\eta). \tag{8}$$

We denote $\mathcal{Q}_v^\eta$ as the number of nonzero entries at a location v and its neighborhood, and then $\alpha_{\mathcal{Q}_v^\eta}$ is the set of components lied in the neighbor of the coefficient α_v^η. From Bayesian probability theory, the prior and posterior are referred to as conjugate distributions when the prior and the posterior distributions belong to a common family. Based on the fact that Beta distribution is conjugate to Bernoulli likelihood, we assume γ_v^η to follow the Beta distribution, Beta(e^η, f^η), with e^η and f^η denoting the hyper-parameters. Notice that the values of e^η and f^η play a significant role in the developed algorithm. The Beta(e^η, f^η) distribution tends to draw a small value of γ_v^η if $e^\eta < f^\eta$, and a large value if $e^\eta > f^\eta$, while it exerts a non-informative prior if $e^\eta = f^\eta$. As a result, by setting appropriate values of e^η and f^η, we can encourage or discourage the continuity of the pixel under test. Detailed discussion about the choice of hyper-parameters e^η and f^η can be found in [25].

C. PRIOR ON NOISE PRECISION

For the sake of facilitating the inference of the noise precision, a Gamma distribution is assumed on β^η, which is expressed as

$$p(\beta^\eta) = \text{Gamma}(\beta^\eta|e_0^\eta, f_0^\eta) \tag{9}$$

where e_0^η and f_0^η are the model parameters.

Algorithm 1 The Proposed Structure-Aware Bayesian SAR Imaging Algorithm

Input: Input the observation data $\mathbf{r}$ and the dictionary Θ.

1: Initialize the latent variables $\mathbf{k} = \{\mathbf{d}, \mathbf{g}\}$, parameters $\mathcal{M} = (\boldsymbol{\sigma}, \boldsymbol{\gamma}, \beta)$, hyper-parameters $\mathcal{H} = \{a, b, e, f, e_0, f_0\}$; set δ, J_{iter}.
2: **while** $\|\mathbf{d}^{(j)} - \mathbf{d}^{(j-1)}\|_2/\|\mathbf{d}^{(j)}\|_2 < \delta$ or $j < J_{\text{iter}}$ **do**
3: Update latent variables $\mathbf{k} = \{\mathbf{d}, \mathbf{g}\}$ using (17) and (20);
4: Update unknown parameters $\mathcal{M} = \{\boldsymbol{\sigma}, \boldsymbol{\gamma}, \beta\}$ using (21), (22) and 23);
5: **end while**

Output: The final image $\boldsymbol{\alpha} = \mathbf{d} \odot \mathbf{g}$.

III. STRUCTURE-AWARE BAYESIAN SAR IMAGING ALGORITHM

A. BAYESIAN INFERENCE

Given the measurement vector $\mathbf{r}$ (we omit the superscript η in this section for simplicity), the complete probabilistic description of the SAR image formation over all hidden variables is described as

$$\begin{aligned} p(\boldsymbol{\alpha}, \boldsymbol{\sigma}, \boldsymbol{\gamma}, \beta|\mathbf{r}, \mathcal{H}) \propto\ & p(\mathbf{r}|\Theta\boldsymbol{\alpha}, \beta) \cdot p(\mathbf{d}|\boldsymbol{\sigma}) \cdot p(\boldsymbol{\sigma}|a, b) \\ & \cdot p(\mathbf{g}|\boldsymbol{\gamma}) \cdot p(\boldsymbol{\gamma}|e, f) \cdot p(\beta|e_0, f_0) \end{aligned} \tag{10}$$

where we denote $\mathcal{H} = \{a, b, e, f, e_0, f_0\}$ as the hyper-parameters. Due to the analytical estimation has not been found for $(\boldsymbol{\alpha}, \boldsymbol{\sigma}, \boldsymbol{\gamma}, \beta)$, therefore, the variational Bayesian inference (VBI) is adopted in this paper to carry out the inference of posteriors.

By calculating the integration over the latent variables $\mathbf{k} = \{\mathbf{d}, \mathbf{g}\}$ and the parameters set $\mathcal{M} = \{\boldsymbol{\sigma}, \boldsymbol{\gamma}, \beta\}$, we obtain the complete marginal probability of the observed data

$$p(\mathbf{r}|\mathcal{H}) = \int p(\mathbf{k}, \mathbf{r}, \mathcal{M}|\mathcal{H}) d\mathbf{k} d\mathcal{M}. \tag{11}$$

In the variational method, this problem is addressed by using the approximate distributions $q(\mathbf{k})$ and $q(\mathcal{M})$ to approximate the intractable posterior $p(\mathbf{k})$ and $p(\mathcal{M})$. (11) is rewritten in log likelihood as

$$\begin{aligned} \ln p(\mathbf{r}|\mathcal{H}) =\ & \mathcal{Z}\left(q(\mathbf{k}), q(\mathcal{M})\right) \\ & + \mathcal{D}_{KL}\left(q(\mathbf{k})q(\mathcal{M})||p(\mathbf{k}, \mathcal{M}|\mathbf{r}, \mathcal{H})\right) \end{aligned} \tag{12}$$

in which

$$\mathcal{Z}(q(\mathbf{k}), q(\mathcal{M})) = \int q(\mathbf{k})q(\mathcal{M}) \ln \frac{p(\mathbf{k}, \mathcal{M}, \mathbf{r}|\mathcal{H})}{q(\mathbf{k})q(\mathcal{M})}$$

and $\mathcal{D}_{KL}$ is the Kullback-Leibler (KL) divergence [22] between the true posterior and the approximated one, which takes the form

$$\begin{aligned} &\mathcal{D}_{KL}\left(q(\mathbf{k})q(\mathcal{M})||p(\mathbf{k}, \mathcal{M}|\mathbf{r}, \mathcal{H})\right) \\ &\quad = \arg\min_{q(\mathbf{k})q(\mathcal{M})} \int q(\mathbf{k})q(\mathcal{M}) \ln \frac{q(\mathbf{k})q(\mathcal{M})}{p(\mathbf{k}, \mathcal{M}|\mathbf{r}, \mathcal{H})} d\mathbf{k} d\mathcal{M}. \end{aligned}$$

It follows that $\mathcal{Z}(q(\mathbf{k}), q(\mathcal{M}))$ is a rigorous lower bound for $\ln p(\mathbf{r}|\mathcal{H})$. In addition, because the left-hand side of (12) is

independent to $q(\mathbf{k})$ and $q(\mathcal{M})$, maximizing $\mathcal{Z}(q(\mathbf{k}), q(\mathcal{M}))$ with respect to $q(\mathbf{k})$ and $q(\mathcal{M})$ equals to minimize $\mathcal{D}_{KL}$, thus $q(\mathbf{k})$ and $q(\mathcal{M})$ stand for an approximation to the posterior distribution $p(\mathbf{k}, \mathcal{M}|\mathbf{r}, \mathcal{H})$. By performing some derivations [22], it is concluded that VBI involves a two-stage procedure. In one stage, the rules for updating the hidden variables $\mathbf{k}$ are given on the basis of the approximate posterior $q(\mathbf{k})$. Using the fact that $q(\mathbf{k}) = \sum_{v=1}^{MN} q(k_v)$, we obtain the posterior for each hidden variable as

$$\ln q^{(j+1)}(k_v) \propto \langle \ln p(k_v, \mathbf{r}|\mathcal{M}, \mathcal{H})\rangle_{q^{(j)}(\mathcal{M})}. \tag{13}$$

In the other stage, the update rules for the parameters $\mathcal{M}$ are given by

$$\ln q^{(j+1)}(\mathcal{M}) \propto \ln p(\mathcal{M}|\mathcal{H}) + \langle \ln p(\mathbf{k}, \mathbf{r}|\mathcal{M}, \mathcal{H})\rangle_{q^{(j+1)}(\mathbf{k})} \tag{14}$$

where $\langle\cdot\rangle_{q(\mathbf{k})}$ accounts for the expectation with respect to $q(\mathbf{k})$, and j is the iterative index.

The posterior $q(\mathbf{d})$ is evaluated by calculating the term of $\ln q(\mathbf{d})$ that depends on $\mathbf{d}$:

$$\begin{aligned}\ln q(\mathbf{d}) \propto\ & \langle \ln p(\mathbf{r}|\boldsymbol{\Theta}, \mathbf{d}, \mathbf{g}, \beta)\rangle_{q(\beta)q(\mathbf{g})} \\ & + \left\langle \sum_{v=1}^{MN} \ln p(d_v|\sigma_v)\right\rangle_{q(\sigma_v)}.\end{aligned} \tag{15}$$

It turns out that the variational distribution for $\mathbf{d}$ is Gaussian $q(\mathbf{d}) = \mathcal{CN}(\mathbf{d}|\boldsymbol{\mu}, \boldsymbol{\Lambda})$, in which the posterior mean value $\boldsymbol{\mu}$ and covariance $\boldsymbol{\Lambda}$ are respectively given by

$$\boldsymbol{\mu} = \langle\beta\rangle\boldsymbol{\Lambda}\langle\mathbf{G}\rangle\boldsymbol{\Theta}^H\mathbf{r} \tag{16a}$$

$$\begin{aligned}\Lambda = \Big\{\langle\beta\rangle\Big[\boldsymbol{\Theta}^H\boldsymbol{\Theta} \odot \Big(\langle\mathbf{g}\rangle\langle\mathbf{g}\rangle^H + \mathrm{diag}\left(\langle\mathbf{g}\rangle \odot (1 - \langle\mathbf{g}\rangle)\right)\Big)\Big] \\ + \langle\Sigma\rangle\Big\}^{-1}\end{aligned} \tag{16b}$$

where $\mathbf{G} = \mathrm{diag}(g_1, ..., g_{MN})$. Consequently, the rule for updating $\mathbf{d}$ is derived as follows

$$\langle\mathbf{d}\rangle = \boldsymbol{\mu}. \tag{17}$$

As for the updating rule for $\mathbf{g}$, we first evaluate the probability for $g_v = 1$, which takes the form

$$\ln p(g_v = 1) \propto \langle \ln \boldsymbol{\gamma}\rangle - \langle\beta\rangle\left(\left\langle d_v^2\right\rangle\boldsymbol{\theta}_v^H\boldsymbol{\theta}_v - 2\langle d_v\rangle\boldsymbol{\theta}_v^H\mathbf{r}_{\neg v}\right) \tag{18}$$

where $\langle d_v^2\rangle = \langle d_v\rangle^2 + \Lambda_{(v,v)}$. Then we obtain that the probability for $g_v = 0$ is proportional to

$$\ln p(g_v = 0) \propto \langle \ln(1 - \gamma_v)\rangle. \tag{19}$$

Therefore, $\mathbf{g}$ can be updated by

$$\langle g_v\rangle = \frac{p(g_v = 1)}{p(g_v = 0) + p(g_v = 1)}. \tag{20}$$

We next update the precision parameter σ_v. $q(\sigma_v)$ is found to be a Gamma distribution, $\mathrm{Gamma}(\sigma_v|\hat{a}_v, \hat{b}_v)$, with $\hat{a}_v = a + 1$ and $\hat{b}_v = b + \langle d_v^2\rangle = b + \mu_v^2 + \Lambda_{(v,v)}$. Hence, the mean of σ_v is expressed as

$$\langle\sigma_v\rangle = \hat{a}_v/\hat{b}_v. \tag{21}$$

Working in a similar manner for each element of $\boldsymbol{\gamma}$, given the updated value for $\mathbf{g}$, the posterior of γ_v can be computed as $q(\gamma_v) \propto \mathrm{Beta}(\gamma_v|\hat{e}, \hat{f})$, where $\hat{e} = e + \alpha_{\mathcal{Q}_v}$ and $\hat{f} = f + |\mathcal{Q}_v| - \alpha_{\mathcal{Q}_v}$. As a result, we obtain

$$\langle \ln \gamma_v\rangle = \varpi\left(\hat{e}\right) - \varpi\left(\hat{e} + \hat{f}\right) \tag{22a}$$

$$\langle \ln (1 - \gamma_v)\rangle = \varpi\left(\hat{f}\right) - \varpi\left(\hat{e} + \hat{f}\right) \tag{22b}$$

where $\varpi(\cdot)$ denotes a digamma function [25].

Finally, we compute the variational distribution of the noise precision β as $q(\beta) = \mathrm{Gamma}(\beta|\hat{e}_0, \hat{f}_0)$, where $\hat{e}_0 = e_0 + L$, and $\hat{f}_0 = f_0 + \left\langle\|\mathbf{r} - \Theta(\mathbf{d} \odot \mathbf{g})\|^2\right\rangle_{q(\mathbf{d})q(\mathbf{g})}$. Consequently, the mean of β is

$$\langle\beta\rangle = \hat{e}_0/\hat{f}_0. \tag{23}$$

B. STOPPING CRITERION

Algorithm 1 summarizes the developed algorithm. Due to the fact that the convergence of VBI is guaranteed, the latent variables and parameters of the proposed algorithm can be updated iteratively until convergence. Iterations are stopped if a maximum number of iteration J_{iter} is reached, or the convergence criterion $\|\mathbf{d}^{(j)} - \mathbf{d}^{(j-1)}\|_2/\|\mathbf{d}^{(j)}\|_2 < \delta$ is achieved, where $\delta > 0$ is a prefixed small value.

C. COMPUTATIONAL COMPLEXITY

In the current form, the main computation load of the proposed algorithm lies in the calculation of the matrix inverse in (16b). Its computational complexity is in the order of $\mathcal{O}\left((MN)^3 \times J_{\mathrm{iter}}\right)$. This can be problematic in the practical application, because MN might be quite large in cases of large target scene. To address this shortcoming, we use the matrix inverse lemma, thus (16b) can be calculated as [20]

$$\begin{aligned}\Lambda = & \langle\mathbf{W}\rangle^{-1} - \langle\mathbf{W}\rangle^{-1}\langle\Theta\rangle^H(1/\langle\beta\rangle\mathbf{I} \\ & + \langle\Theta\rangle\langle\mathbf{W}\rangle^{-1}\langle\Theta\rangle^H)^{-1}\langle\Theta\rangle\langle\mathbf{W}\rangle^{-1}\end{aligned} \tag{24}$$

in which $\langle\mathbf{W}\rangle = \langle\beta\rangle\mathrm{diag}(\langle\mathbf{g}\rangle \odot (1 - \langle\mathbf{g}\rangle) \odot (\Theta^H\Theta)) + \langle\Sigma\rangle$ and $\langle\Theta\rangle = \Theta\langle\mathbf{G}\rangle$. Since $\langle\mathbf{W}\rangle$ is a diagonal matrix, the inverse can be easily calculated via inverting its diagonal elements. Consequently, computational complexity of the proposed algorithm is reduced to $\mathcal{O}((L^3 + MN \times L^2 + (MN)^2 \times L) \times J_{\mathrm{iter}})$. Using the fact that $L < MN$, we can further written the computational complexity of the proposed algorithm in the order of $\mathcal{O}((MN)^2 \times L \times J_{\mathrm{iter}})$.

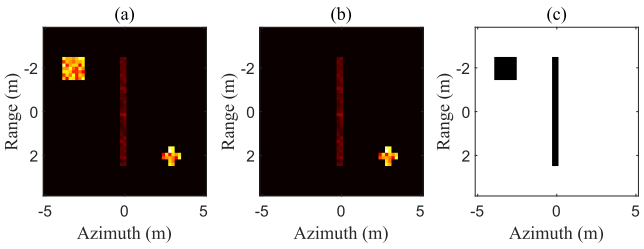

FIGURE 1. The synthetic scene. (a),(b) Time-1 and Time-2 amplitude images; (c) true change map.

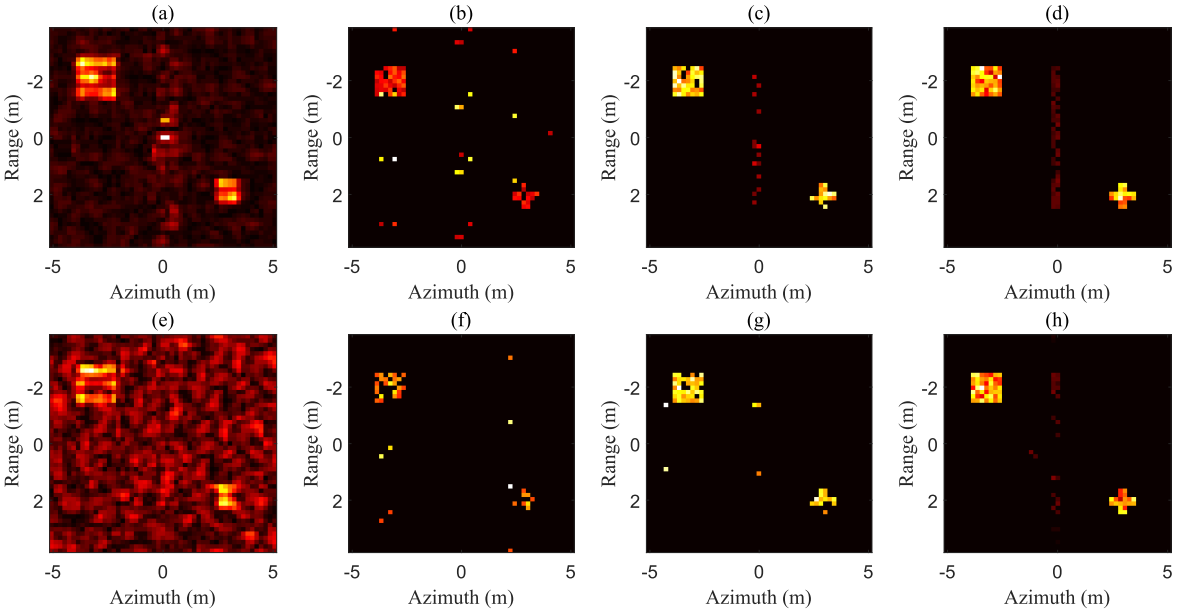

FIGURE 2. Time-1 amplitude images of synthetic scene (SNR = 15 dB) using 1/4 of the measurements by (a) PFA; (b) CoSaMP; (c) GS; (d) proposed method. Time-1 amplitude images of synthetic scene (SNR = 15 dB) using 1/8 of the measurements by (e) PFA; (f) CoSaMP; (g) GS; (h) proposed method.

IV. NUMERICAL EXPERIMENTS

In this section, numerical simulations are conducted to evaluate the performance of the proposed algorithm in comparison with other reported ones. Algorithms tested include polar format algorithm (PFA) [26], CoSaMP [10], GS [13] and the proposed method. Similar as [27], the measure of change for pixel v is estimated using the sample coherence estimator:

$$\pi_v = \frac{2|\sum_{i\in\mathcal{Q}_v} \alpha_i^s(\alpha_i^t)^*|}{(\sum_{i\in\mathcal{Q}_v}|\alpha_i^s|^2)+(\sum_{i\in\mathcal{Q}_v}|\alpha_i^t|^2)} \tag{25}$$

where α_i^s and α_i^t are pixels in neighborhood $\mathcal{Q}_v$ of the vth pixel. π_v will approach to unity if no-change occurs, and it will belong to (0, 1) in a change case.

Firstly, the synthetic data experiment is carried out, where the synthetic scene consists of two different changes. One is the obvious amplitude change and the other is phase-only change, with both representing continuity structures. The original reference and mission scenes are respectively depicted in Fig. 1(a) and (b). The locations of the induced change are shown in Fig. 1(c), where the rectangle indicates the locations of amplitude changes, and the straight path represents the locations of phase changes. Table 1 lists the radar setup. The frequency bandwidth B is 1 GHz so that the ideal range resolution is $c/2B = 0.15$m, where c is the speed of light. The angular range $\Delta\theta$ is set to be 5° and the azimuth resolution is calculated as $\lambda/2\Delta\theta = 0.2$m. The target scene of interest is of size $7.6 \times 10\text{m}^2$. The amplitudes of the scattering centers distribute as a complex Gaussian whose mean is 2.0 and variance is 0.5. The observation data is corrupted by the complex Gaussian noise with signal-to-noise ratio (SNR) of 15 dB. Interrupt data is realized by randomly sampling in the range and azimuth domains under different interrupted ratios from the reference and mission pass collections.

TABLE 1. Radar setup for simulated data.

Parameter	Value
Center frequency f_c	9 GHz
Frequency bandwidth B	1 GHz
Angular range $\Delta\theta$	5°
Size of the scene MN	51×51 pixels

Fig. 2 shows the different Time-1 imaging results using 1/4 and 1/8 of the full measurements, respectively. As displayed in Fig. 2(a), the PFA image is seriously blurred. In Fig. 2(b), many scatterers are missing in the image obtained by CoSaMP while some artificial points are observed outside the target region. Because the sparsity-driven-based regularization is capable of denoising, the GS result shown in Fig. 2(c) performs better than CoSaMP. However, GS does not obtain a very satisfactory image in the case of gapped data. This is reasonable, since the noise rejection process of GS to achieve a relatively sparse and clear target scene might cause the elimination of some scatterers with low amplitudes. In contrast, the devised approach performs well by taking advantage of the continuity structures of the target, as depicted in Fig. 2(d), where the scatterers with relatively low amplitudes are effectively retained and the background noise is removed. When only 1/8 measurements are available, the PFA image shows worse performance as shown in Fig. 2(e). Fig. 2(f) and (g) give the CoSaMP and GS results, respectively, in which the reconstructed points are fewer than the developed one shown in Fig. 2(h), with more

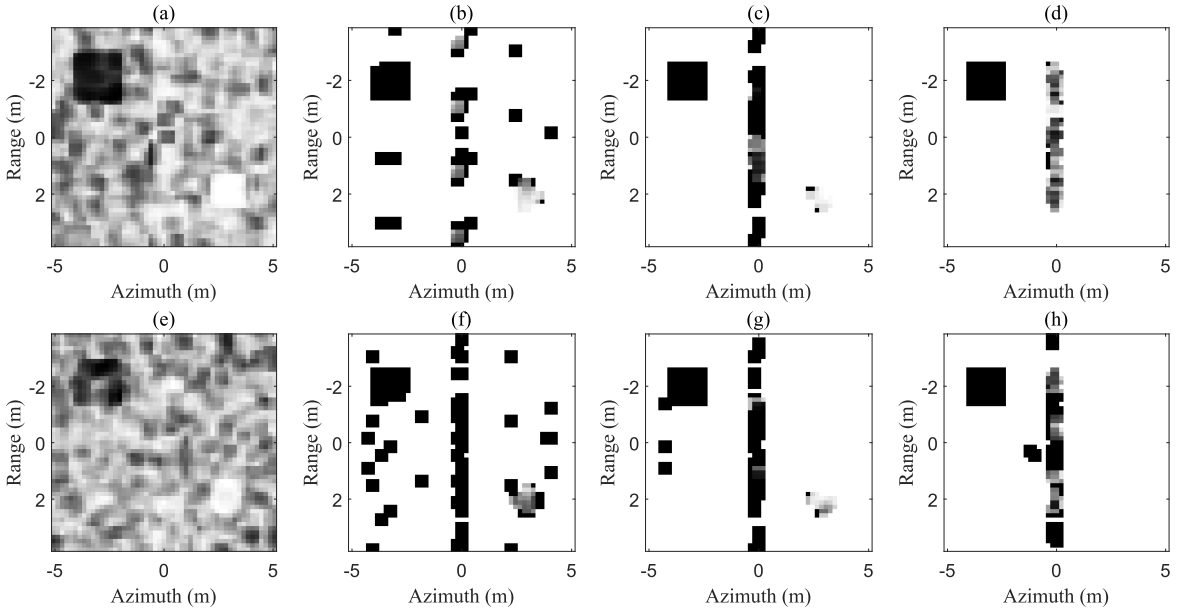

FIGURE 3. Change detection results of synthetic scene (SNR = 15 dB) using 1/4 of the measurements by (a) PFA; (b) CoSaMP; (c) GS; (d) proposed method. Change detection results of synthetic scene (SNR = 15 dB) using 1/8 of the measurements by (e) PFA; (f) CoSaMP; (g) GS; (h) proposed method.

TABLE 2. RMSE against interrupted ratio.

Interrupted Ratio	PFA	CoSaMP	GS	Proposed
1/4	-5.6714	-8.3568	-8.9517	-11.5267
1/8	-4.4546	-7.2583	-8.0748	-10.9402

TABLE 3. Average coherence against interrupted ratio.

Interrupted Ratio	PFA	CoSaMP	GS	Proposed
1/4	0.6936	0.8884	0.8995	0.9157
1/8	0.6826	0.8336	0.8931	0.8989

weak scatterers missed. Fig. 3 shows the corresponding CCD results of Fig. 2. The coherence estimator (25) is applied to the paired image reconstructions. In comparison, the devised algorithm can further promote the continuity property of the target, thus a better CCD result is achieved.

The quality of reconstruction for different methods is measured besides the visual results. The relative mean squared error (RMSE) is adopted as the recovery performance metric, defined by $\text{RMSE} = \frac{1}{F}\sum_{f=1}^{F} 20 * \log_{10}\left(||\mathbf{r} - \hat{\mathbf{r}}_f||_2/||\mathbf{r}||_2\right)$, where F denotes the total number of independent Monte Carlo trials and $\hat{\mathbf{r}}_f$ is the fth reconstructed data. The RMSEs of the imaging results using various algorithms corresponding to the used number of data is provided in Table 2. It is seen that the RMSEs of all algorithms consistently decrease as the number of measurements increases. The proposed algorithm achieves the smallest RMSEs among all the benchmark ones. Another performance metric is the average coherence between the recovered paired images. Table 3 displays the average coherence values of the compared approaches. In accord with Fig. 3, the proposed scheme achieves higher CCD performance than other methods.

To further verify the proposed method, the data provided by the X-band GOTCHA SAR dataset is used. From the dataset, we choose the same spatial region of images FP0120 and

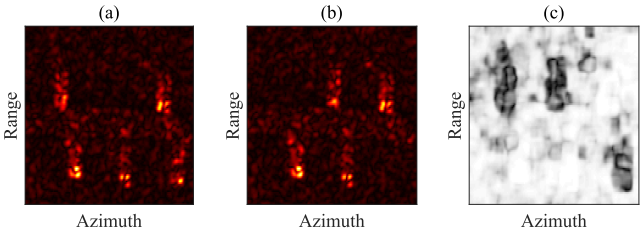

FIGURE 4. The GOTCHA imagery. (a), (b) Time-1 and Time-2 amplitude images; (c) complete-data CCD benchmark image.

FP0124 as Time-1 reference scene and Time-2 mission pass scene. Fig. 4(a) and (b) show the amplitude images of the scene at these two different observation time. Fig. 4(c) calculates the value of π_v for the complete-data image, and acts as a benchmark. Interrupted data is obtained by deleting the samples of the full measurement according to a 1/2 random gap pattern. Then the Gaussian noise is added into the gapped data by setting the SNR as 20 dB. The imaging and CCD results obtained by different methods are presented in Fig. 5. It is observed that the results achieved by the proposed approach are superior among these methods. By making full use of the structure-aware priors and deriving the VBI algorithm, the devised approach has the ability of learning the algorithm parameters directly from measurement, hence achieving the performance gain of change detection.

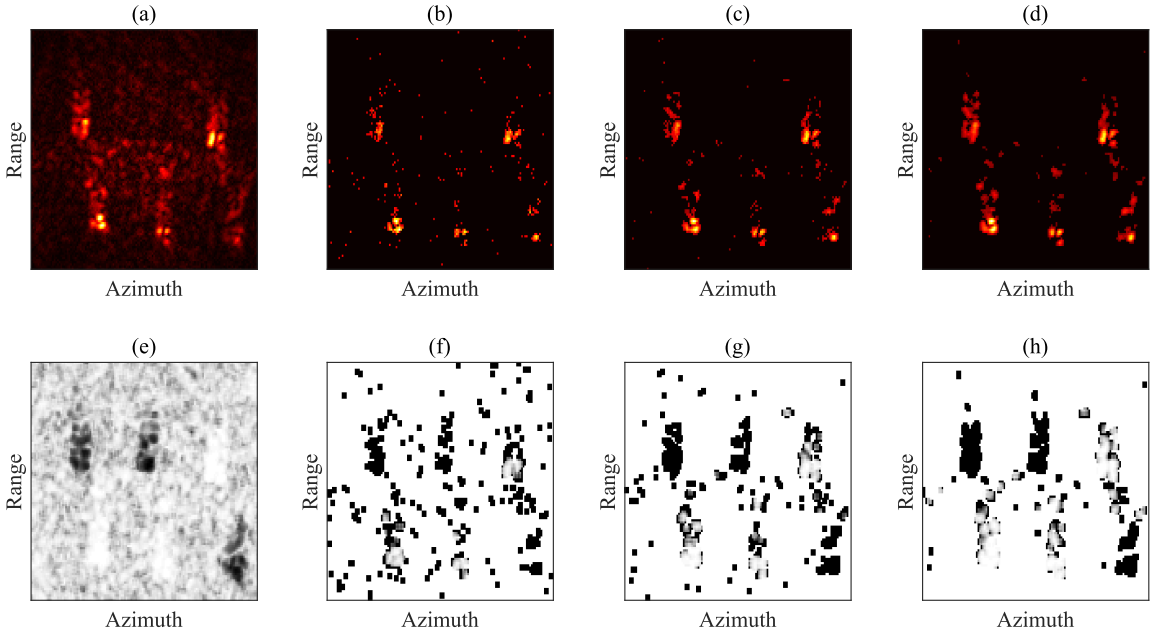

FIGURE 5. Time-1 amplitude images of GOTCHA imagery (SNR = 20 dB) using 1/2 of the measurements by (a) PFA; (b) CoSaMP; (c) GS; (d) proposed method. Change detection results using 1/2 of the measurements by (e) PFA; (f) CoSaMP; (g) GS; (h) proposed method.

V. CONCLUSION

This work proposed an efficient interrupted SAR image formation scheme in Bayesian formalism with application to persistent surveillance SAR imaging. A hierarchical Bayesian model is first developed to characterize the continuity structures of the target scene. Then the VBI algorithm is adopted to reconstruct multi-pass data collections with missing samples, followed by the change detection estimator applied on the resulting SAR images. Experiments indicate that the proposed approach achieves a significant performance enhancement, by which the scatterers on the target are well preserved and the artificial points are efficiently removed. It also exhibits superiority over other existing approaches on the imaging results by the RMSE criterion, and on the change detection results in terms of the average coherence.

REFERENCES

[1] J. Salzman, D. Akamine, R. Lefevre, and J. C. Kirk, "Interrupted synthetic aperture radar (SAR)," *IEEE Aerosp. Electron. Syst. Mag.*, vol. 17, no. 5, pp. 33–39, May 2002.

[2] J. A. Bruder and R. Schneible, "Interrupted SAR waveforms for high interrupt ratios," in *Proc. IET Int. Conf. Radar Syst.*, Oct. 2007, pp. 1–5.

[3] E. G. Larsson and J. Li, "Spectral analysis of periodically gapped data," *IEEE Trans. Aerosp. Electron. Syst.*, vol. 39, no. 3, pp. 1089–1097, Jul. 2003.

[4] D. L. Donoho, "Compressed sensing," *IEEE Trans. Inf. Theory*, vol. 54, no. 4, pp. 1289–1306, Apr. 2006.

[5] S. S. Chen, D. L. Donoho, and M. A. Saunders, "Atomic decomposition by basis pursuit," *SIAM Rev.*, vol. 43, no. 1, pp. 129–159, 2001.

[6] R. Tibshirani, "Regression shrinkage and selection via the lasso," *J. Roy. Statist. Soc., B (Methodol.)*, vol. 58, no. 1, pp. 267–288, 1996.

[7] I. F. Gorodnitsky and B. D. Rao, "Sparse signal reconstruction from limited data using FOCUSS: A re-weighted minimum norm algorithm," *IEEE Trans. Signal Process.*, vol. 45, no. 3, pp. 600–616, Mar. 1997.

[8] Y. Yang, X. Cong, G. Gui, K. Long, Z. Huang, and Q. Wan, "Polarimetric object-level SAR imaging method with canonical scattering characterisation by exploiting joint sparsity," *IET Radar Sonar Navigat.*, vol. 11, no. 10, pp. 1558–1566, Oct. 2017.

[9] Y. C. Pati, R. Rezaiifar, and P. S. Krishnaprasad, "Orthogonal matching pursuit: Recursive function approximation with applications to wavelet decomposition," in *Proc. 27th Asilomar Conf. Signals, Syst. Comput.*, Nov. 1993, pp. 40–44.

[10] D. Needell and J. A. Tropp, "CoSaMP: Iterative signal recovery from incomplete and inaccurate samples," *Appl. Comput. Harmon. Anal.*, vol. 26, no. 3, pp. 301–321, 2009.

[11] I. Stojanovic, L. Novak, and W. C. Karl, "Joint reconstruction of interrupted SAR imagery for persistent surveillance change detection," *Proc. SPIE*, vol. 8746, no. 1, pp. 1–9, May 2013.

[12] I. Stojanovic, W. C. Karl, and L. Novak, "Reconstruction of interrupted SAR imagery for persistent surveillance change detection," *Proc. SPIE*, vol. 8394, no. 8, pp. 1–16, May 2012.

[13] I. Stojanovic, L. Novak, and W. C. Karl, "Interrupted SAR persistent surveillance via group sparse reconstruction of multipass data," *IEEE Trans. Aerosp. Electron. Syst.*, vol. 50, no. 2, pp. 987–1003, Apr. 2014.

[14] Y. C. Eldar, P. Kuppinger, and H. Bolcskei, "Block-sparse signals: Uncertainty relations and efficient recovery," *IEEE Trans. Signal Process.*, vol. 58, no. 6, pp. 3042–3054, Jun. 2010.

[15] M. Yuan and Y. Lin, "Model selection and estimation in regression with grouped variables," *J. Roy. Statist. Soc., B (Statist. Methodol.)*, vol. 68, no. 1, pp. 49–67, 2006.

[16] J. Fang, Y. Shen, H. Li, and P. Wang, "Pattern-coupled sparse Bayesian learning for recovery of block-sparse signals," *IEEE Trans. Signal Process.*, vol. 63, no. 2, pp. 360–372, Jan. 2013.

[17] J. Fang, L. Zhang, and H. Li, "Two-dimensional pattern-coupled sparse Bayesian learning via generalized approximate message passing," *IEEE Trans. Image Process.*, vol. 25, no. 6, pp. 2920–2930, Jun. 2016.

[18] L. Wang, L. Zhao, G. Bi, C. Wan, and L. Yang, "Enhanced ISAR imaging by exploiting the continuity of the target scene," *IEEE Trans. Geosci. Remote Sens.*, vol. 52, no. 9, pp. 5736–5750, Sep. 2014.

[19] L. Yu, H. Sun, J. P. Barbot, and G. Zheng, "Bayesian compressive sensing for cluster structured sparse signals," *Signal Process.*, vol. 92, pp. 259–269, Jan. 2012.

[20] L. Yu, C. Wei, J. Jia, and H. Sun, "Compressive sensing for cluster structured sparse signals: Variational Bayes approach," *IET Signal Process.*, vol. 10, no. 7, pp. 770–779, Sep. 2016.

[21] Y. Yang, X. Cong, K. Long, Y. Luo, W. Xie, and Q. Wan, "MRF model-based joint interrupted SAR imaging and coherent change detection via variational Bayesian inference," *Signal Process.*, vol. 151, pp. 144–154, Oct. 2018.
[22] D. G. Tzikas, A. C. Likas, and N. P. Galatsanos, "The variational approximation for Bayesian inference," *IEEE Signal Process. Mag.*, vol. 25, no. 6, pp. 131–146, Jan. 2008.
[23] K. E. Themelis, A. A. Rontogiannis, and K. D. Koutroumbas, "A variational Bayes framework for sparse adaptive estimation," *IEEE Trans. Signal Process.*, vol. 62, no. 18, pp. 4723–4736, Sep. 2014.
[24] J. A. Jackson and R. L. Moses, "Synthetic aperture radar 3D feature extraction for arbitrary flight paths," *IEEE Trans. Aerosp. Electron. Syst.*, vol. 48, no. 3, pp. 2065–2084, Jul. 2012.
[25] L. Yu, H. Sun, G. Zheng, and J. P. Barbot, "Model based Bayesian compressive sensing via local beta process," *Signal Process.*, vol. 108, pp. 259–271, Mar. 2015.
[26] S. Quegan, "Spotlight synthetic aperture radar: Signal processing algorithms," *J. Atmos. Solar-Terr. Phys.*, vol. 59, no. 5, pp. 597–598, 1995.
[27] M. Cha, R. D. Phillips, P. J. Wolfe, and C. D. Richmond, "Two-stage change detection for synthetic aperture radar," *IEEE Trans. Geosci. Remote Sens.*, vol. 53, no. 12, pp. 6547–6560, Dec. 2015.

YI GAN received the B.S. degree from the School of Computer Science and Engineering, University of Electronic Science and Technology of China (UESTC), Chengdu, China, in 2002, and the M.S. degree in electronic and communication engineering from UESTC, in 2012. He is currently with The 10th Research Institute of CETC, Chengdu. His research interests include radar signal processing, information fusion, and passive detection.

XUNCHAO CONG was born in Sichuan, China. He received the Ph.D. degree from the School of Electronic Engineering, University of Electronic Science and Technology of China (UESTC), Chengdu, China, in 2017. He is currently with The 10th Research Institute of CETC, Chengdu. His research interests include radar signal processing, radio localization, and information fusion.

YUE YANG (S'15) was born in Sichuan, China. She received the B.Eng. degree from the School of Electronic Engineering, University of Electronic Science and Technology of China, Chengdu, China, in 2015, where she is currently pursuing the Ph.D. degree with the School of Information and Communication Engineering. Since 2019, she has been a Visiting Student with the Department of Electrical and Computer Engineering, National University of Singapore, Singapore. Her research interests include synthetic aperture radar imaging, sparse signal reconstruction, and statistical signal processing.